Available online at www.eccomasproceedia.org
Eccomas Proceedia SMART (2023) 1768-1777

ECCOMAS
Proceedia

X ECCOMAS Thematic Conference on Smart Structures and Materials
SMART 2023
D.A. Saravanos, A. Benjeddou, N. Chrysochoidis and T. Theodosiou (Eds)

PARAMETER IDENTIFICATION AND MODELING OF SUPERELASTIC SHAPE MEMORY ALLOY WIRES SUBJECTED TO DYNAMIC LOADS

NIKLAS LENZEN*, SVEN KLINKEL* AND OKYAY ALTAY*

*Chair of Structural Analysis and Dynamics
RWTH Aachen University
Mies-van-der-Rohe-Str. 1, 52074 Aachen, Germany
e-mail: lenzen@lbb.rwth-aachen.de

Key words: shape memory alloys, superelastic, constitutive model, machine learning, feedforward neural networks, parameter identification

Abstract. In this study, we combine classical macroscopic modeling with machine learning to determine the relevant material parameters for the superelastic response modeling of shape memory alloy (SMA) wires. Our goal is to accurately map cyclic stress responses to corresponding material parameters. Due to their versatile structure, we focus on feedforward neural networks (FNNs). Several parameters representing the critical stress, entropy, internal energy, and thermodynamic behavior of SMA wires are identified. In this approach, the searched parameters are sampled within a predefined parameter space using the Latin hypercube sampling method. The parameter sets, together with strain loading, are then applied to the constitutive model to generate the corresponding stress responses for the training of an FNN. After training, the network can identify the model parameters from conventional cyclic tensile stress–strain tests. The method is validated by comparing the numerical results with experimental data.

1 INTRODUCTION

Shape memory alloys (SMAs) are two-phase polycrystalline metals, which exhibit superelastic response if the material is in an austenitic steady state. When subjected to dynamic loading, energy is dissipated during the repeated phase transformations from austenite to martensite and *vice versa*. Besides their exceptional energy dissipation potential, SMAs show further unique characteristics, such as large deformation recovery, corrosion resistance, and low fatigue. Thus, SMA-based vibration control devices have been a particular area of research in civil engineering. A review and detailed summary of the related applications can be found in [1, 2].

The design of SMA-based control devices requires accurate constitutive models. Due to their numerical efficiency, macroscopic models are generally preferred. For an efficient heat transfer, most control devices are equipped with SMAs as wires and require uniaxial models in particular. As a consequence, many one-dimensional thermodynamically-coupled constitutive models have been proposed, such as in [3, 4]. Various improvements to these models have also been proposed,

Peer-review under responsibility of the organizing committee of SMART 2023.
doi: 10.7712/150123.9947.444214

such as in [5, 6]. A detailed review of constitutive models and modeling techniques for SMAs can be found in [7], and references therein.

The accurate response modeling of constitutive SMA models depends on the choice of material parameters. Therefore, experiments are necessary, such as mechanical and thermomechanical tests. For SMA wires, uniaxial tensile tests are sufficient to obtain stress–strain relations. Whereas the parameter identification of thermodynamic properties requires further equipment and techniques, such as thermomechanical analysis or more specifically the differential scanning calorimetry [8, 9]. Another crucial aspect is the fact that even with perfectly determined parameters, constitutive models may need an additional tuning step for accurate response calculations.

To circumvent theses challenges, machine learning methods, in particular *feedforward neural networks* (FNNs), can offer efficient and versatile solutions. According to the universal approximation theorem [10], FNNs are capable of predicting highly nonlinear relations with any desired degree of accuracy and have already been used for solving inverse problems. In the scope of parameter identification, Yagawa and Okuda proposed the application of an FNN to predict the parameters of a material model [11]. Furthermore, for superelastic SMAs subjected to quasi-static loading, Helm identified model parameters using a three-layered FNN with stress histories as inputs [12]. The FNN was trained on numerically generated data. The utilized constitutive model relied on parameters that were randomly sampled within a predefined space.

In this paper, we present an FNN-based parameter identification approach for superelastic SMAs subjected to dynamic loading [13] and expand it for the rate-dependent constitutive SMA model of Auricchio et al. [3]. Besides thermodynamic parameters, the method is now applied to identify also parameters representing the critical stresses, entropy, and internal energy from stress-strain responses. As part of the methodology, the parameters are already tuned after identification and can be directly used by the constitutive model for response calculations.

The remainder of the paper is organized as follows: In Section 2, the method is presented and implemented in combination with the macroscopic model. In Section 3, the method is applied to SMA wires and validated by stress–strain experiments. The conclusions of the study are presented in Section 4.

2 METHODOLOGY

2.1 Superelastic SMA response

SMAs are characterized by two crystalline phase states; austenite (A) and martensite (M). For material temperatures above the austenite transformation finish temperature A_f, the parent phase is austenite, and SMAs exhibit superelastic behavior. High mechanical stresses induce a forward-phase transformation (AM), whereby the SMA crystals reorient their atomic lattice from body centred (B2) to a monoclinic (B19) lattice, which is more stable at high stresses. During unloading, a reverse-phase transformation (MA) occurs, returning the material to its initial shape with no residual deformation. In both forward- and reverse-phase transformations, SMAs undergo pseudoplastic deformations, which are observed by stress plateaus in the stress–strain response. The AM transformation is an exothermic process. The lattice reorientation causes internal heating, which is transferred to the environment through heat convection and conduction. Conversely, the MA transformation is a highly endothermic process, whereby the austenite formation is accompanied by a reduction in material temperature.

Dynamic loading patterns typically involve high strain rates, which affect the release of the heat generated during the AM transformation. This influences the material response such that the slope of the stress plateau increases as the austenite phase is more energetically stable for higher temperatures. As a consequence, the reverse transformation is initiated at higher critical stress levels, which affects the stress–strain curve and the associated hysteretic energy dissipation.

To illustrate the influence of strain rate, experimentally determined SMA wire stress–strain responses are depicted in Figure 1. The SMA composition of the wire is Ni-55.8%-Ti-43.95%. The wire is of length $l = 150$ mm and diameter $d = 0.2$ mm. A pre-stress of $\sigma_0 = 134.9$ MPa is applied. The ambient temperature is $T_0 = 296.2$ K (23.05 °C), while the austenite transformation finish temperature of the wire is $A_f = 285.2$ K (12.05 °C). Accordingly, a superelastic response of the SMA is expected. After training, two cyclic loading histories are applied with strain rate amplitudes of $\dot{\varepsilon}_a = 1.26\%\ \mathrm{s}^{-1}$ and $\dot{\varepsilon}_b = 50.27\%\ \mathrm{s}^{-1}$. Due to high strain rates, the generated heat cannot be released directly and causes a steeper slope of the AM transformation. At high strain rates, the MA transformation is also reshaped and starts earlier at a higher stress level with a steeper slope.

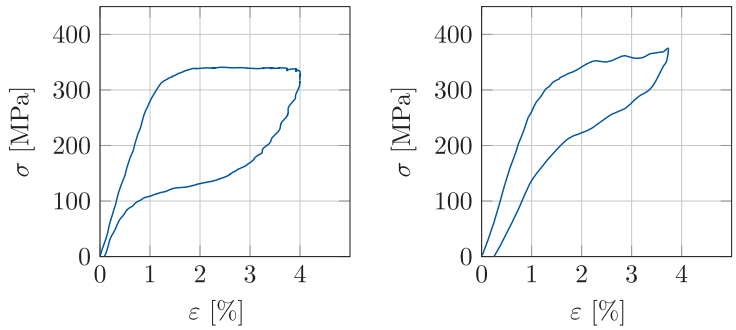

Figure 1: Cyclic tensile tests applied on a superelastic SMA wire after training. Strain rate amplitudes are (**a**) quasi-static $\dot{\varepsilon}_a = 1.26\%\ \mathrm{s}^{-1}$ and (**b**) dynamic $\dot{\varepsilon}_b = 50.27\%\ \mathrm{s}^{-1}$.

2.2 Constitutive modeling of superelastic SMA wire response

The uniaxial thermo-mechanical time-continuous constitutive model by Auricchio et al. [3] is based on a set of external and internal variables. In particular, the uniaxial strain ε as well as the absolut temperature T represent the external variables, whereas the martensite volume fraction ξ refers to the internal variable. The free energy is computed by

$$\begin{aligned}\psi = &\left[(u_A - T\eta_A) - \xi\left(\Delta u - T\Delta\eta\right)\right] + C\left[(T - T_0) - T\ln\frac{T}{T_0}\right] \\ &+ \frac{1}{2}E\left[\varepsilon - \varepsilon_l\xi\ \mathrm{sgn}\left(\sigma\right)\right]^2 - (T - T_0)\left[\varepsilon - \varepsilon_l\xi\ \mathrm{sgn}\left(\sigma\right)\right]E\alpha,\end{aligned} \tag{1}$$

where u_A and η_A are the internal energy and entropy of the austenite phase. Δu and $\Delta\eta$ are the internal energy difference and the entropy difference between the austenite and martensite

phases. C and T_0 are the material heat capacity and the ambient temperature, respectively. E and ε_l are the Young's modulus and the maximum strain at $\xi = 1$, respectively. $\operatorname{sgn}(\cdot)$ is the *signum* function. α is the thermal expansion factor.

The Young's modulus is expressed according to Auricchio and Sacco [14] as a function of the martensite volume fraction to enable a transition between the two phases as

$$E = \frac{E_A E_M}{E_M + \xi\,(E_A - E_M)}, \tag{2}$$

where E_A and E_M are constants representing the associated elastic moduli of the austenite and martensite phases, respectively.

The heat equation is derived from the *first law of thermodynamics* as

$$\begin{aligned} C\dot{T} &= -\frac{\partial \psi}{\partial \xi}\dot{\xi} + T\frac{\partial^2 \psi}{\partial T \partial \varepsilon}\dot{\varepsilon} + T\frac{\partial^2 \psi}{\partial T \partial \xi}\dot{\xi} - \gamma(T - T_0) \\ &= T\left(-E\alpha\dot{\varepsilon} + \left[\Delta\eta + E\alpha\varepsilon_l\,\operatorname{sgn}(\sigma)\right]\dot{\xi}\right) + \left(\Delta u - T\Delta\eta + \varepsilon_l|\sigma|\right)\dot{\xi} - \gamma(T - T_0), \end{aligned} \tag{3}$$

where γ is the heat convection coefficient. The stress response of the SMA wire corresponds to

$$\sigma = \frac{\partial \psi}{\partial \varepsilon} = E\left[\varepsilon - \varepsilon_l \xi\,\operatorname{sgn}(\sigma) - \alpha\,(T - T_0)\right]. \tag{4}$$

The evolution of the martensite fraction ξ is expressed through the following first-order differential equations

$$\text{A} \to \text{M}: \qquad \dot{\xi} = \beta^{AM}\,(1 - \xi)\,\frac{\dot{F}}{\left(F - R_f^{AM}\right)^2}\mathcal{H}^{AM}, \tag{5}$$

$$\text{M} \to \text{A}: \qquad \dot{\xi} = \beta^{MA}\xi\frac{\dot{F}}{\left(F - R_f^{MA}\right)^2}\mathcal{H}^{MA}, \tag{6}$$

where F is the driving force, $R_f^{AM/MA}$ are the thermo-coupled limit stress levels, and $\beta^{AM/MA}$ are the speed parameters controlling the rate of transformation. Moreover, the terms $\mathcal{H}^{AM/MA}$ are defined as the activation factors relative to the austenite-to-martensite and martensite-to-austenite transformations, respectively, and are expressed by

$$\mathcal{H}^{AM} = \begin{cases} 1 & \text{when } \dot{F} > 0 \text{ and } R_s^{AM} < F < R_f^{AM}, \\ 0 & \text{otherwise}, \end{cases} \tag{7}$$

$$\mathcal{H}^{MA} = \begin{cases} 1 & \text{when } \dot{F} < 0 \text{ and } R_f^{MA} < F < R_s^{MA}, \\ 0 & \text{otherwise}, \end{cases} \tag{8}$$

where

$$F = |\sigma| - T\frac{\Delta\eta}{\varepsilon_l}, \tag{9}$$

$$R_{s/f}^{AM/MA} = \sigma_{s/f}^{AM/MA} - T_0\frac{\Delta\eta}{\varepsilon_l}. \tag{10}$$

Here, $\sigma_{s/f}^{AM/MA}$ are critical stress levels at which the phase transformations start/finish at T_0.

Particularly for the dynamic response modeling, these parameters are hard to identify as they are interacting with each other. For example, as can be seen in Equations (5,6) and (10), there is a direct relation between the speed parameters, critical stresses, and entropy difference, so that these parameters have to be adjusted with respect to each other.

2.3 Feedforward neural network based parameter identification

The macroscopic SMA model computes the stress response σ, temperature T, and martensite volume fraction ξ using strain ε and strain rate $\dot{\varepsilon}$ as input. Accordingly, the model can be expressed as $\mathcal{M}\left(\left(\boldsymbol{\varepsilon}, \dot{\boldsymbol{\varepsilon}}\right), \mathbf{p}\right)$, where the vectors $\boldsymbol{\varepsilon}$ and $\dot{\boldsymbol{\varepsilon}}$ are time histories of strain and strain rate, respectively. The vector $\mathbf{p}$ contains mechanical, thermodynamical and phenomenological parameters, that need to be determined from experiments. Furthermore, for accurate response modeling, particularly for the determination of the phenomenological parameters, an additional parameter tuning step is necessary. In this study, both the thermodynamical experiments as well as the parameter tuning step are replaced by a machine learning based procedure that utilizes an FNN to identify the searched parameters from cyclic tensile stress–strain experiments.

The procedure consists of two steps: data generation and parameter identification. As shown in Figure 2(a), the data set $\mathcal{D}$ for training the FNN is generated using the constitutive model from Section 2.2. The searched parameters $\mathbf{p}_i, \forall i \in \{1:N\}$ are sampled from a predefined parameter space using the *Latin hypercube sampling* method [15], where N is the number of samples. In total, ten parameters are searched representing the critical stress levels $\sigma_{s/f}^{AM/MA}$, internal energy difference Δu, entropy difference $\Delta\eta$, heat capacity C, heat convection coefficient γ, and speed parameters $\beta^{AM/MA}$. Each sampled parameter set $\mathbf{p}_i$ together with strain $\boldsymbol{\varepsilon}_i \in \mathbb{R}^{n\times 1}$ and strain rate $\dot{\boldsymbol{\varepsilon}}_i \in \mathbb{R}^{n\times 1}$ vectors, where n is the number of time instants, are then applied to the constitutive model to generate the corresponding stress response vector $\boldsymbol{\sigma}_i \in \mathbb{R}^{n\times 1}$. As a result, the training data sets $\mathcal{D} = \left\{\left(\boldsymbol{\sigma}_i, \mathbf{p}_i\right), \forall i \in \{1:N\}\right\}$ are obtained.

As illustrated in Figure 2(b), the parameter identification step is established by the trained FNN. The the output of the first hidden layer $\mathbf{p}^{(1)}$ and the output of the final layer $\mathbf{p}^{(l)}$ are

$$\mathbf{p}^{(1)} = f^{(1)}(\mathbf{W}^{(1)\top}\boldsymbol{\sigma}_{\mathrm{EXP}} + \mathbf{b}^{(1)}), \qquad \mathbf{p}^{(l)} = \hat{\mathbf{p}} = f^{(l)}(\mathbf{W}^{(l)\top}\mathbf{p}^{(l-1)} + \mathbf{b}^{(l)}), \tag{11}$$

where $l-1$ is the number of hidden layers, f is the activation function, $\mathbf{W}$ is the weight matrix, $\boldsymbol{\sigma}_{\mathrm{EXP}}$ is the measured stress input vector from experiments, and $\mathbf{b}$ is the bias vector. The vector $\hat{\mathbf{p}}$ contains the parameters predicted by the FNN.

3 RESULTS AND DISCUSSION

3.1 Stress–strain experiments

For test data generation, cyclic tensile tests were conducted on the Ni-55.8%-Ti-43.95% (wire length $l = 150$ mm, diameter $d = 0.2$ mm). The tests were conducted at an ambient temperature around $T_0 = 296.2$ K (23.05°C). Moreover, a pre-stress of $\sigma_0 = 134.9$ MPa was applied. Further information on the test setup can be taken from [16]. All material parameters provided by the manufacturer are reported in Table 1, where E_M, E_A, and ε_l are determined from stress–strain tests under a quasi-static load.

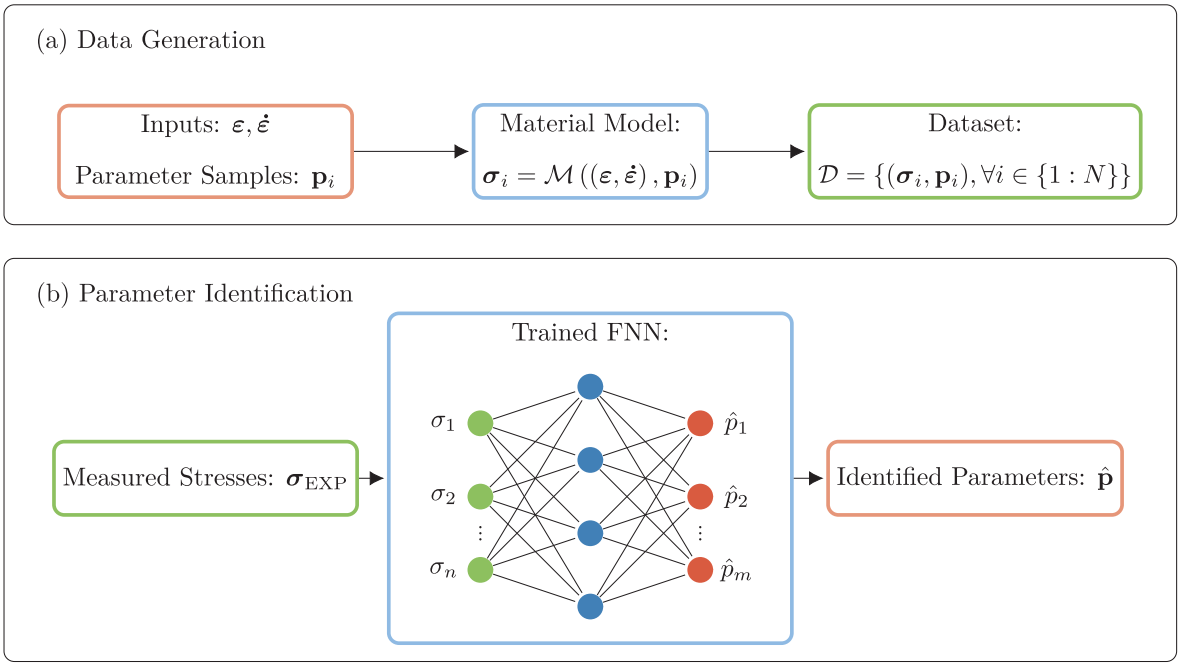

Figure 2: (**a**) Data generation step: Parameter samples $\mathbf{p}_i$ are fed into the material model to produce the corresponding stress outputs $\boldsymbol{\sigma}_i$. (**b**) Parameter identification step: The trained FNN estimates the searched parameters $\hat{\mathbf{p}}$ from experimental stress–strain response.

3.2 Parameter identification

For the parameter identification, a four-layered FNN is utilized, where each layer contains 128 neurons. The *hyperbolic tangent* activation function is used in the hidden layers, whereas the *sigmoid* function is applied in the final layer scaling the outputs between 0 and 1. Additionally, to avoid vanishing gradients and overfitting, the *batch normalization* [17] and the *dropout* [18] algorithms are applied. For training, the *mean squared error function* and the *Adam optimizer* [19] with a learning rate of $1 \cdot 10^{-3}$ are used. The FNN is trained for 500 epochs and a batch size of $1 \cdot 10^4$. The training data set $\mathcal{D}$ is composed of $2 \cdot 10^4$ parameter sets $\mathbf{p}_i$, which are sampled from a predefined parameter space, and the corresponding stress responses $\boldsymbol{\sigma}_i$. The parameter space is listed in Table 2, where the parameters are alternated around the reference setting according to previous studies [3, 5]. As a result, the data set $\mathcal{D} = \{(\boldsymbol{\sigma}_i, \mathbf{p}_i), \forall i \in \{1 : 2 \cdot 10^4\}\}$ is generated, of which 10% are used for validation. For greater stability against measurement errors, a *Gaussian noise* with zero mean and a variance of $1 \cdot 10^{-4}$ is added to the training input data.

To consider strain rate effects, the data set is generated for three different stain rate amplitudes of $\dot{\varepsilon} \in [12.57, 25.13, 50.27]\%\ \mathrm{s}^{-1}$ with a strain amplitude of $\varepsilon = 4\%$. Figure 3 illustrates for 10 sampled parameter sets the corresponding stress response range computed by the constitutive model ($\dot{\varepsilon} = 25.13\%\ \mathrm{s}^{-1}$, $\varepsilon = 4\%$). The large deviation of the responses demonstrate the effects of parameter sets.

After training, the tensile stress–strain experiments are conducted within the same strain and

Table 1: Known parameters of the investigated SMA wires.

Parameter		Value	Unit
Young's modulus of martensite	E_M	14100	MPa
Young's modulus of austenite	E_A	29000	MPa
Maximum strain at $\xi = 1$	ε_l	0.04	-
Thermal expansion factor	α	0.0	-
Ambient temperature	T_0	296.2	K
Diameter	d	0.02	mm
Wire length	l	150	mm

Table 2: Sample space of the searched parameters $\mathbf{p}_i$.

Parameter		min	max	Unit
AM transformation start stress	σ_s^{AM}	85	170	MPa
AM transformation finish stress	σ_f^{AM}	350	600	MPa
MA transformation start stress	σ_s^{MA}	200	350	MPa
MA transformation finish stress	σ_f^{MA}	70	200	MPa
Internal energy difference	Δu	0	100	MPa
Entropy difference	$\Delta\eta$	0.0	0.3	MPa K^{-1}
Heat capacity	C	0.1	10.0	MPa K^{-1}
Speed parameter of the AM transformation	β^{AM}	1	10	-
Speed parameter of the MA transformation	β^{MA}	1	100	-
Heat convection coefficient	γ	0	10	-

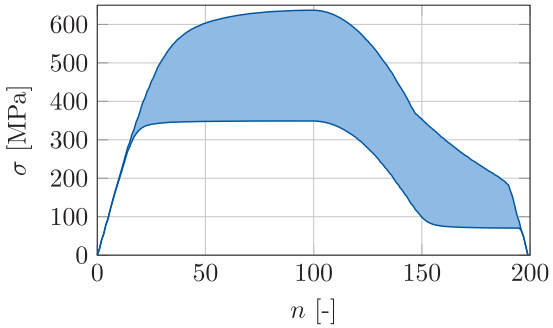

Figure 3: Stress response range covered by 10 sampled parameter sets $\mathbf{p}_i$, $\forall i \in \{1 : 10\}$ for ($\dot{\varepsilon} = 25.13\%\ s^{-1}$, $\varepsilon = 4\%$). Each response signal contains $n = 200$ data points.

strain rate amplitude range. The stress responses are divided into 200 equidistantly distributed points. Table 3 lists the identified parameters with respect to each strain rate. The final parameter values are determined from the mean over all investigated strain rate cases.

Table 3: Parameters $\hat{\mathbf{p}}$ estimated by the FNN from measured stress responses corresponding to strain rate amplitudes $\dot{\varepsilon} \in [12.57, 25.13, 50.27]\%\ \mathrm{s}^{-1}$ and strain amplitude of $\varepsilon = 4\%$.

Parameter	$\dot{\varepsilon} = 12.57\ [\%\,\mathrm{s}^{-1}]$	$\dot{\varepsilon} = 25.57\ [\%\,\mathrm{s}^{-1}]$	$\dot{\varepsilon} = 50.27\ [\%\,\mathrm{s}^{-1}]$	Final result $\hat{\mathbf{p}}$
σ_s^{AM}	85.11	85.08	85.08	85.09
σ_f^{AM}	350.47	353.90	350.67	351.68
σ_s^{MA}	329.82	319.54	299.71	316.36
σ_f^{MA}	79.25	79.38	79.09	79.24
Δu	74.78	75.59	76.33	75.57
$\Delta\eta$	0.087	0.088	0.089	0.088
C	2.28	2.34	2.48	2.37
γ	3.12	3.14	3.04	3.10
β^{AM}	2.88	2.90	3.27	3.02
β^{MA}	92.74	94.29	94.66	93.90

In Figure 4, the experimental results are compared with the numerical calculations, which use the identified parameter set $\hat{\mathbf{p}}$. The numerical calculations accurately map the dynamic behavior of the experimental results for both the loading and unloading path. It is worth noting, that the accuracy of the parameter identification method is limited by the precision of the constitutive model. Here, effects, such as residual deformations and hardening, are not included in the constitutive model. Therefore, these effects cannot be covered in the parameter identification process.

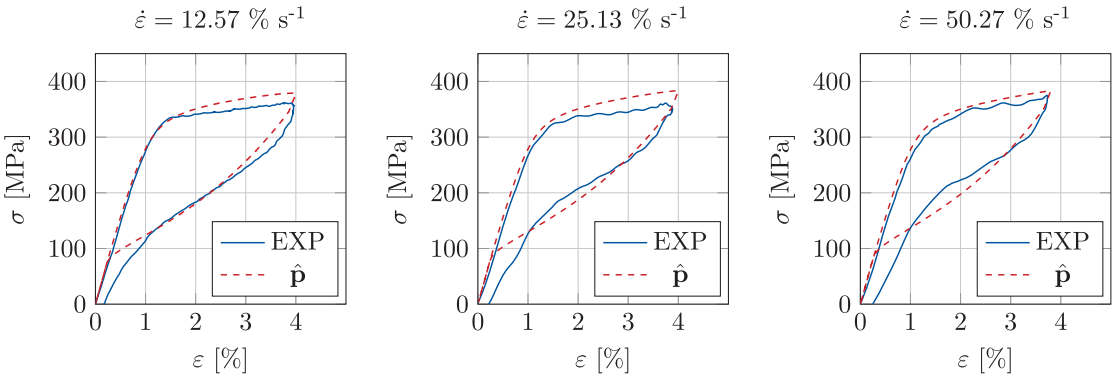

Figure 4: Comparison of the experimentally determined stress–strain responses (EXP) with numerical calculations using the identified parameter set $\hat{\mathbf{p}}$.

4 CONCLUSIONS

In this paper, an FNN-based methodology was presented for superelastic SMA wires for the identification and tuning of mechanical, thermodynamical and phenomenological parameters. In an initial step, training data were generated using a constitutive model. Therefore, the searched parameters were sampled within a predefined parameter space, which were then used to compute the corresponding stress responses. After training, the FNN identified the searched parameters from cyclic tensile stress–strain tests. Finally, the accuracy of the proposed method was validated by comparing the numerical results with experimental data.

References

[1] C. Fang and W. Wang, *Shape Memory Alloys for Seismic Resilience*. Springer, 2020.

[2] A. Tabrizikahou, M. Kuczma, M. Łasecka-Plura, E. N. Farsangi, M. Noori, P. Gardoni, and S. Li, "Application and modelling of shape-memory alloys for structural vibration control: State-of-the-art review," *Construction and Building Materials*, vol. 342, p. 127975, 2022.

[3] F. Auricchio, D. Fugazza, and R. Desroches, "Rate-dependent thermo-mechanical modelling of superelastic shape-memory alloys for seismic applications," *Journal of Intelligent Material Systems and Structures*, vol. 19, no. 1, pp. 47–61, 2008.

[4] S. Zhu and Y. Zhang, "A thermomechanical constitutive model for superelastic SMA wire with strain-rate dependence," *Smart Materials and Structures*, vol. 16, no. 5, p. 1696, 2007.

[5] A. Kaup, O. Altay, and S. Klinkel, "Macroscopic modeling of strain-rate dependent energy dissipation of superelastic sma dampers considering destabilization of martensitic lattice," *Smart Materials and Structures*, vol. 29, no. 2, p. 025005, 2019.

[6] A. Kaup, H. Ding, J. Wang, and O. Altay, "Strain rate dependent formulation of the latent heat evolution of superelastic shape memory alloy wires incorporated in multistory frame structures," *Journal of Intelligent Material Systems and Structures*, vol. 32, no. 11, pp. 1198–1214, 2021.

[7] Z. Wang, J. Luo, W. Kuang, M. Jin, G. Liu, X. Jin, and Y. Shen, "Strain rate effect on the thermomechanical behavior of niti shape memory alloys: A literature review," *Metals*, vol. 13, no. 1, p. 58, 2022.

[8] D. Depriester, A. Maynadier, K. Lavernhe-Taillard, and O. Hubert, "Thermomechanical modelling of a NiTi SMA sample submitted to displacement-controlled tensile test," *International Journal of Solids and Structures*, vol. 51, no. 10, pp. 1901–1922, 2014.

[9] Y. Xiao, P. Zeng, L. Lei, and H. Du, "Experimental investigation on rate dependence of thermomechanical response in superelastic niti shape memory alloy," *Journal of Materials Engineering and Performance*, vol. 24, pp. 3755–3760, 2015.

[10] K. Hornik, M. Stinchcombe, and H. White, "Multilayer feedforward networks are universal approximators," *Neural networks*, vol. 2, no. 5, pp. 359–366, 1989.

[11] G. Yagawa and H. Okuda, "Neural networks in computational mechanics," *Archives of Computational Methods in Engineering*, vol. 3, pp. 435–512, 1996.

[12] D. Helm, "Pseudoelasticity: experimental observations, thermomechanical modeling, and identification of the material parameters," in *Smart Structures and Materials 2004: Active Materials: Behavior and Mechanics*, vol. 5387. SPIE, 2004, pp. 198–209.

[13] N. Lenzen and O. Altay, "Machine learning enhanced dynamic response modelling of superelastic shape memory alloy wires," *Materials*, vol. 15, no. 1, p. 304, 2022.

[14] F. Auricchio and E. Sacco, "A one-dimensional model for superelastic shape-memory alloys with different elastic properties between austenite and martensite," *International Journal of Non-Linear Mechanics*, vol. 32, no. 6, pp. 1101–1114, 1997.

[15] M. D. McKay, R. J. Beckman, and W. J. Conover, "A comparison of three methods for selecting values of input variables in the analysis of output from a computer code," *Technometrics*, vol. 42, no. 1, pp. 55–61, 2000.

[16] A. Kaup, O. Altay, and S. Klinkel, "Strain amplitude effects on the seismic performance of dampers utilizing shape memory alloy wires," *Engineering Structures*, vol. 244, p. 112708, 2021.

[17] S. Ioffe and C. Szegedy, "Batch normalization: Accelerating deep network training by reducing internal covariate shift," in *International Conference on Machine Learning*. JMLR: W&CP, 2015, pp. 448–456.

[18] N. Srivastava, G. Hinton, A. Krizhevsky, I. Sutskever, and R. Salakhutdinov, "Dropout: a simple way to prevent neural networks from overfitting," *The Journal of Machine Learning Research*, vol. 15, no. 1, pp. 1929–1958, 2014.

[19] D. P. Kingma and J. Ba, "Adam: A method for stochastic optimization," *arXiv preprint arXiv:1412.6980*, 2014.